

CONGENITAL HEART DISEASE

Anatomical Assessment of Congenital Heart Disease

John C. Wood, MD, PhD

Department of Pediatrics and Radiology, Keck School of Medicine, Children's Hospital of Los Angeles, Los Angeles, California, USA

ABSTRACT

Cardiac MRI (CMR) is replacing diagnostic cardiac catheterization as the modality of choice for anatomic and functional characterization of congenital heart disease (CHD) when echocardiographic imaging is insufficient. In this manuscript, we discuss the principles of anatomic imaging of CHD, placing emphasis on the appropriate choice and modification of pulse sequences necessary to evaluate infants and small children. Clinical examples are provided to illustrate the relative strengths and shortcomings of different CMR imaging techniques. Although cardiovascular function and flow techniques are not described, their role in evaluating the severity of anatomic defects is emphasized. Anatomic characterization represents the first component of a carefully-planned, integrated CMR assessment of CHD.

INTRODUCTION

Two-dimensional echocardiography is the diagnostic mainstay for congenital heart disease (CHD) because of its portability, ease of use, and excellent tempero-spatial resolution. Cardiac anatomy and physiology are sufficiently well described by echocardiogram that many patients proceed straight to surgery without additional imaging (1). However, echocardiography may be limited by poor acoustic windows in some patients. In particular, extracardiac structures such as the great arteries and great veins may be difficult to profile. Complex intracardiac connections such as interatrial baffles or superior-inferior ventricles may also be difficult to resolve by ultrasound. Historically, diagnostic cardiac catheterization was indicated when lesion location or severity could not adequately be visualized by echocardiography. However, cardiac magnetic resonance imaging (CMR) can now often answer unresolved anatomic questions noninvasively. The ability to image in arbitrary planes is com-

plemented by true 3-dimensional angiography to yield superior anatomic and functional data for both intracardiac and extracardiac structures.

CMR for children with congenital heart disease (CHD) is challenging because of the tremendous diversity of cardiac malformations and associated defects. This complexity precludes a purely cook-book approach to scanning these patients. With that said, a *systematic* approach is essential, analogous to segmental techniques used in ultrasonography. The goals of CMR in patients with CHD are three-fold:

1. characterize location and anatomic severity of primary lesion;
2. assess functional consequences of primary lesion;
3. identify both associated and incidental defects.

The first goal is relatively straightforward; image cardiac defects in multiple planes such that the reviewer can gain a visual impression of their hemodynamic significance. The most useful anatomic pulse sequences and their advantages and disadvantages will be discussed in this manuscript.

The second goal refers to qualitative or quantitative measures of lesion significance. For example, left ventricular mass is one metric of left-sided obstruction severity. Similarly, the ratio of pulmonary to systemic blood flow reflects the severity of left-to-right shunts such as ventricular septal defects. In parallel hemodynamic circuits, such as the pulmonary arteries or veins, quantitative flow measurements may be more important than the assessments of stenosis severity than peak velocities. Pulse sequences for functional and flow analysis will be discussed in other chapters.

Received 2 August 2005; accepted 30 November 2005.

Correspondence to:

John C. Wood, MD, PhD

Department of Pediatrics and Radiology

Keck School of Medicine

Children's Hospital of Los Angeles

Los Angeles, CA 90027-0034

USA

email: jwood@chla.usc.edu

The third goal simply reflects the complexity of these patients. Even patients that have had comprehensive cardiac evaluations and surgery may have incomplete or incorrect diagnoses. CMR is not limited by acoustic or surgical windows and may unveil new diagnoses or interpretations. CMR protocol planning for new patients should therefore include enough “big picture” imaging to identify previously unsuspected abnormalities.

One would never take a patient to the catheterization laboratory without a careful review of the patient’s history and relevant laboratory and imaging data. In contrast, such detailed information is rarely obtained prior to performing a 2D echocardiogram. The demands of the MRI suite represent an intermediate to these extremes. Details of previously identified anatomic findings derived from prior clinic, echocardiogram, surgical or catheterization reports are extremely helpful, although the logistics of this varies considerably with referral source. In some cases, direct review of the echocardiogram is warranted. A chest X-ray, if available, should be reviewed for the presence of clips, coils, stents, and pacemakers. Patients with late return of atrioventricular node function may forget that they have a pacemaker. Retained temporary pacing wires should also be excluded by chest X-ray in postoperative patients.

Perhaps the most important preparatory step in planning the MRI examination is determining the *specific* question to be answered. For example, when a patient is referred for coarctation evaluation, the referring physician wants to know whether to do nothing, to refer for surgery or to attempt intervention in the catheterization laboratory. This mindset must be maintained when planning the imaging protocol. With its multiple modalities, CMR is ideally suited for anatomic-functional correlations. Lastly, CHD patients often have multiple cardiac abnormalities. While each lesion might deserve attention in its own right, some lesions may have already been well characterized by other modalities. Communication with the referring physician is essential.

In this article, we provide a general framework for anatomic characterization of CHD. We start by outlining the “imaging toolbox,” although a more detailed description of relevant pulse sequences and imaging techniques is provided by Dr. Simonetti. Next, exam planning and execution are discussed. Lastly, a series of examples illustrating the scope of CMR anatomical imaging is provided.

METHODOLOGY

Although there are dozens of cardiac pulse sequences for anatomic imaging, many with manufacturer-specific features, they can crudely be broken down into 3 classes:

1. black-blood imaging;
2. white-blood cine imaging;
3. 3D gadolinium-enhanced angiography

Sequences for evaluating functional parameters such as tissue-strain, blood velocity, oxygen saturation, and myocardial perfusion will not be systematically discussed in this article (2–5).

Black-blood imaging

Black-blood images have high signal-to-noise ratio (SNR), resolution, and contrast. Most techniques use radiofrequency refocusing, making them robust to metal artifact. This is particularly important in post-operative patients where surgical clips would otherwise cause local image voids and anatomic disruption. Black-blood techniques have greatest utility when the relationships between airway and vessels must be elucidated (6). They are also vital for characterizing masses, thrombi, abdominal situs, hematomas or other soft tissue details (7).

Standard spin echo techniques

Once a workhorse of CMR, we only use standard spin echo when SNR is paramount and respiratory artifacts are low, particularly in term and premature infants. Heart rates are generally > 120 beats per minute (bpm) in these patients, lowering T1 contrast and decreasing the number of available slices. To correct for this, we generally gate on every other R-wave for heart rates over 140 bpm. Some platforms only support respiratory compensation, not respiratory triggering. These algorithms may require an even number of averages; we typically use 4 excitations, leading to an exam time of 5–8 minutes. Inadequate blood nulling can be problematic in coronal and sagittal planes, particular in straight vessels like the aorta and vena cavae.

Fast spin echo (FSE) techniques

In fast spin echo, image collection is accelerated by a factor of the echo train length (ETL), enabling single slice acquisition in a breath-hold. Since each phase encoding is collected at a different portion of the cardiac cycle, ETL must be kept relatively short to avoid blurring. ETL must also be lowered as heart rate increases. A useful rule of thumb is to adjust ETL to keep the image acquisition time for a single slice between 12 and 16 seconds. Fast spin echo techniques are not inherently “black-blood” so they are often used in conjunction with some sort of inversion pulse to null the blood pool. Default value of the inversion time is around 650 ms but varies with heart rate. The inversion time needs to be significantly shortened if used after a gadolinium injection.

Fast spin echo techniques are the preferred imaging black-blood imaging modality for all patients who can breath-hold. Respiratory artifact and blurring are problematic in free-breathing patients, particularly fat-ghosts from the moving anterior chest wall. These may be ameliorated by using multiple averages (typically 3) and by placing saturation bands across the anterior chest wall.

White-blood cine imaging

Static pictures can answer many questions in pediatric cardiology but incompletely characterize lesion severity. Any sonographer can relate to the difficulty of interpreting still-frames taken out of their dynamic context. Although cine images in MRI are retrospectively-gated (not real time), they offer the same physiologic context provided by echocardiography. For

this reason, cine images represent the backbone of congenital CMR even though they have lower resolution and contrast than black-blood imaging.

SPGR techniques

SPGR represents the older of the two techniques (8). Its advantages are its robustness and its flow sensitivity. Blood flowing into the imaging plane carries nonsaturated spins and appears bright, yielding the appearance of streamlines even in slow-flowing blood (e.g., pulmonary veins). Blood accelerated to the point of turbulence, however, produces signal voids because of spin randomization. Combined with bright signal from flow convergence below the obstruction, these signal voids highlight hemodynamically significant stenoses. We use SPGR to characterize severity of both valvular and vascular stenoses. SPGR yields best images with breath-holding. However, it works relatively well with either respiratory-triggering or respiratory-averaging (using 2 or 3 signal averages). The primary limitation of SPGR is its relatively poor image contrast and low SNR.

SSFP techniques

SSFP offers many advantages to SPGR. Since spoiling is unnecessary, TR's are roughly 50% shorter, allowing better temporal and spatial resolution during breath-hold imaging. Larger flip angles can also be used, improving SNR. Image contrast is much higher and represents a product of T1 and T2 weighting; this is particularly useful in evaluating the myocardium, masses, and pericardial structures. However, SSFP has largely replaced SPGR for myocardial imaging as well as extracardiac anatomic characterization (9). SSFP has three primary disadvantages. Its ultrashort TE produces less flow sensitivity to vascular or valvular obstructions. More importantly, SSFP is troubled by flow artifacts near regions of rapid blood acceleration (10). These artifacts can be crippling in infants and young children since they have significantly greater blood acceleration in the aorta and great arteries than adults. Local shimming improves but does not eliminate these artifacts. A second limitation of SSFP is that reducing the field of view (FOV) and slice thickness can greatly prolong the echo and repetition times (this is done to reduce the absorbed radiofrequency power and gradient switching rates). Since longer TR and TE degrade image quality and exacerbate flow artifacts, we will often use SSFP with larger field of view and larger matrices than we would with SPGR. Many of these trade-offs between acquisition parameters are vendor and hardware specific and need to be determined empirically.

3D gadolinium-enhanced angiography

Contrast-enhanced magnetic resonance angiography (CEMRA) represents the only true 3D technique available for routine assessment. Since voxels are more isotropic than for 2D acquisitions, images collected by 3D sequences are ideally suited for multiplanar reformatting and volume rendering. CEMRA acquisitions are ungated, so they are only useful for characterization of extracardiac structures. Despite short

acquisition times, CEMRA has high SNR, allowing the highest resolution of any of the cardiac imaging sequences. Although large vessel disease may be well characterized by standard 2D imaging, CEMRA is absolutely essentially for small vessel disease such as peripheral pulmonic stenosis or aortico-pulmonary collaterals (11, 12). In fact, CEMRA offers comparable diagnostic accuracy as cardiac catheterization in evaluating the number and location of aorticopulmonary collaterals in children (11, 13) and adults with pulmonary atresia (12).

Since CEMRA represents an "off-label" use of gadolinium, guidelines for dosing have been derived empirically, particularly for pediatrics. Previous studies have typically used 0.2 mM per kilogram of gadolinium although higher doses have been described (13–15). Hand injection at 0.5–1 cc/second is adequate in infants and small children but a power injection is quite helpful in larger patients. For infants less than 7 kg, we typically dilute the contrast up to a total volume of 3 cc and inject at 0.5 cc/second. All injections should be followed by saline flush of 5–10 cc. Although it appears self-evident, the radiographer must take venous anatomy into account when placing the intravenous line (IV). For example, a lower extremity IV will not opacify the pulmonary arteries in a patient with a Glenn shunt. Bilateral vena cavae are quite common and bilateral upper extremity IVs may be necessary in some patients to evaluate upper extremity venous thromboses or collaterals.

Synchronizing image acquisition to the contrast bolus delivery is important to maximize image quality. Many systems now allow the operator to track contrast progress using a low resolution "fluoro" mode so that the high resolution acquisition can be triggered during maximum contrast enhancement (16). Other systems allow the user to assign a region of interest for automated contrast detection and acquisition triggering. This works relatively well in larger patients but we have not observed consistent performance in infants and small children. Timing boluses can be used to estimate the contrast delivery curve, however injection flow rates and volumes during the test bolus generally differ from those used during actual angiogram. However, reasonable results can still be obtained using empiric knowledge of the pulse sequence and the injection technique/site. Contrast delivery occurs later from lower extremity injection sites, smaller IV's, and in low cardiac output states. Fontan patients, as a result of their expanded venous capacitance, can have remarkably long transit times from the venous injection site to the heart. In contrast, gadolinium delivery through a central line produces almost immediate right-sided opacification.

Synchronization of the bolus and the acquisition requires an understanding of the CEMRA phase ordering; the goal being to co-locate the center of k-space and the contrast. For example, a standard, single average acquisition will acquire the center of k-space in the middle of the acquisition, thus the scanner should ideally be triggered before the peak contrast enhancement. Use of fractional acquisitions will move the center of k-space relatively earlier. There are also numerous techniques for acquiring k-space from the "inside-out." Use of these approaches requires full contrast delivery prior to scan initiation or blood vessels

will appear peripherally bright with central nonenhancement. Given the increased uncertainty of contrast delivery in infants and children, standard rectilinear phase order (full or partial acquisitions) offers the highest probability of success.

The last considerations for CEMRA are the orientation and voxel sizes. Echo and repetition times are shortest in principal planes. Since most 3D acquisitions are post-processed extensively, there is little reason to image in oblique planes. Resolution is highest in the frequency direction, followed by the phase and slice directions; this should be accounted for when considering the “important” questions to be answered by the angiogram. Although the scanner generally interpolates the slice direction by a factor of two or four to yield seemingly isotropic voxels, this does not represent “real” resolution in this direction.

PLANNING AND EXECUTING THE EXAMINATION

The most important “anticipatory” decisions are the choice of sedation (if any), imaging coil, and imaging protocol (including use of contrast) (17). Children under the age of seven will generally require sedation or anesthesia. The use of conscious sedation (such as pentobarbital or chloral hydrate), deep sedation (propofol), or general anesthesia (e.g., isoflurane), varies tremendously from institution to institution depending upon resources. Although general anesthesia with intubation and paralysis is safe and provides a mechanism for breath-hold imaging in younger patients, it is not necessary for the overwhelming majority of anatomic diagnoses (18). We restrict intubation to patients who have vulnerable airways or for diseases where the respiratory artifact will clearly compromise decision-making. The best example of this is pulmonary atresia with multiple aortico-pulmonary collaterals where vessel tracking can be challenging even with a breath-hold angiogram.

Imaging coil choice will also be dictated by local availability. One should always use the smallest coil that provides coverage of the relevant anatomy. Smaller coils have higher SNR, allowing finer resolution and/or faster imaging. For example, we place all neonates <4.5 kg in a knee coil (rather than a head or cardiac coil). This produces a 250% improvement in the SNR, allowing FOV as small as 14 cm. General purpose flexible wrap coils can be used on slightly larger infants, with the head and cardiac coils working well for toddlers through school age. Premature infants may be scanned using small surface coils such as might be used for the wrist or temporo-mandibular joint.

Lastly, it is important to decide upon a general outline for the CMR exam. All exams begin with a series of “localizers,” which tend to be low resolution, ungated images that serve as a starting point for more definitive imaging. Some platforms offer localization based on real time imaging, but this is not universally available. Fast gated or ungated SPGR or SSFP images in two or three principal planes can be performed in 1–2 minutes. We follow these fast initial localizers with gated white blood cine images in the axial plane (SPGR or SSFP), covering the top of the arch to the dome of the diaphragm. Although this is time consuming (4–6 minutes), it generally establishes 90–95% of the

diagnosis and may alert the scanner to abnormalities that were not previously recognized. It is not terribly unusual to modify or discard a carefully-scripted imaging protocol because of new information derived on the “survey” cine sequence.

Subsequent sequences should generally be acquired in order of importance because scans occasionally must be terminated prematurely (mechanical failure, patient instability). If double inversion recovery fast spin echo imaging is going to be used, it is often easier to collect these images prior to any contrast injections. Hence, we tend to collect CEMRAs acquisition last, unless we are also interested in either early or delayed tissue enhancement. Some patients do not need contrast imaging, for example patients with Tetralogy of Fallot who are having serial assessments of right ventricular (RV) size and function. However, CEMRA is such a useful tool that we use it in most of our anatomic assessments.

CLINICAL EXAMPLES

To illustrate the methodologies described above, we will present a series of clinical examples. This is intended to be a diverse sampling of disease states, rather than a didactic presentation of CHD, to illustrate how the techniques elucidate the anatomy and physiology of the lesions. Cases are separated by location, encompassing disorders of the aortic arch, pulmonary arteries, pulmonary veins, systemic veins and intracardiac anatomy. Two examples integrating pathology at multiple levels are also discussed.

Aortic Arch

Case 1: Complex coarctation

CMR has really become a standard-of-care for evaluating the aortic arch as well as arterial-bronchial relationships (6, 19). Figure 1 demonstrates an 11 year old patient with a known vascular ring consisting of a right arch with a left descent and persistent ligamentum. The ligament was divided in infancy but follow-up investigations suggested a 20-torr blood pressure gradient from upper to lower extremity. The purpose of the exam was to determine the level of obstruction. The CMR exam consisted of localizers, axial cine gradient echo images, breath-hold parasagittal double-inversion recovery fast spin echo and cine gradient echo images and a CEMRA in the sagittal plane. Volume rendering of the angiogram (panels A, B) demonstrate successful “release” of the vascular ring (arrows). Black-blood imaging (panel C) demonstrates normal caliber trachea and left bronchus (arrow). The same series indicates a thin, inferior “kink” at the proximal end of the right aortic arch (panel D, arrow). Cine gradient echo images (panel E) demonstrate a systolic, turbulent jet beginning at this kink, but little flow turbulence at the distal junction of the isthmus and descending aorta. The central portion of the jet is bright, indicating flow enhancement without turbulence, but there is signal loss on either side of the central flow acceleration. The degree of obstruction is consistent with the cuff blood pressure gradient and the borderline ventricular hypertrophy observed on the axial cine images (not shown). CEMRA



Figure 1. Patient with left aortic arch and right descent and persistent ligamentum status post ligament division in infancy. A, B) 3D reconstruction of CEMRA in frontal and cranial perspectives. Although there remains a prominent diverticulum of Kommerell, there is wide separation from the left carotid artery (arrows), indicating release of the vascular ring. C) Parasagittal, breath-hold double inversion recovery fast spin echo image demonstrating unobstructed trachea and left bronchus (arrow). D) Parasagittal, breath-hold double inversion recovery FSE image illustrating inferior “kink” (arrow) at proximal end of transverse arch. E) Single systolic frame from SPGR cine images in the same plane, illustrating two systolic signal voids, bracketing central flow related enhancement, beginning at the proximal inferior infolding. F) 3D reconstruction of CEMRA. The transverse arch is seen to be tortuous between the right carotid artery and the descending aorta. Proximal kink (arrow) is unimpressive, likely representing motional averaging.

(panel F) demonstrates long segment isthmus tortuosity and mild hypoplasia. However, the proximal “kink” is not very obvious on the angiogram. The reason for this is that the angiogram is an ungated acquisition, blurring structures that move during the cardiac cycle. Thin structures, such as membranes, folds, or indentations, are particularly vulnerable to being underdiagnosed compared with longer segment obstructions. This effect can be particularly prominent in the pulmonary arteries because they are relatively more distensible than the aorta. Recent work suggests that the best predictors of a clinically-significant (>20 torr) upper-to-lower extremity blood pressure gradient are the minimum aortic cross-sectional area and evidence of flow-delay (assessed by the heart-rate corrected flow deceleration) (20). Aortico-aortic collaterals may decrease or eliminate arm-leg blood pressure differences, but these may be easily assessed by CEMRA and even quantitated by phase contrast measurements (21).

Case 2: Aortic dissection

The previous example represents our standard “arch” protocol. For vascular ring evaluations, we will generally perform black-blood imaging in axial and coronal planes. In older children, SSFP may be substituted for SPGR in some applications. Figure 2 (panels A and B) demonstrates coronal and parasagittal images from an asymptomatic 21-year-old patient with Marfan’s

disease who was status post aortic root replacement 2 years previously. A massive pseudo-aneurysm is seen having an entry point near the base of the innominate artery and a re-entry point distal to the left subclavian artery. Both sluggish and pulsatile blood have high contrast, unlike with SPGR, and there is excellent definition of the intimal dissection. Indeed, the whole diagnosis can essentially be made from these images. However, CEMRA provides a nice three-dimensional overview to the lesion extent and entry point. During the first pass, contrast (panel C) fills the true aorta and the proximal portion of the dissection through the entry point at the base of the innominate artery. A huge intimal dissection compresses the true aortic lumen throughout the transverse arch. The origin of the left subclavian is also distorted, indicating direct extension into this vessel. The second acquisition (panel D, roughly 24 seconds after injection) highlights contrast retention within the massive pseudoaneurysm; head vessels and true arch lumen are relatively less enhanced.

Pulmonary arteries

Case 3: Homograft and left pulmonary artery stenosis

In addition to the evaluation of arch abnormalities, CMR represents a standard-of-care for pulmonary artery evaluation (22).

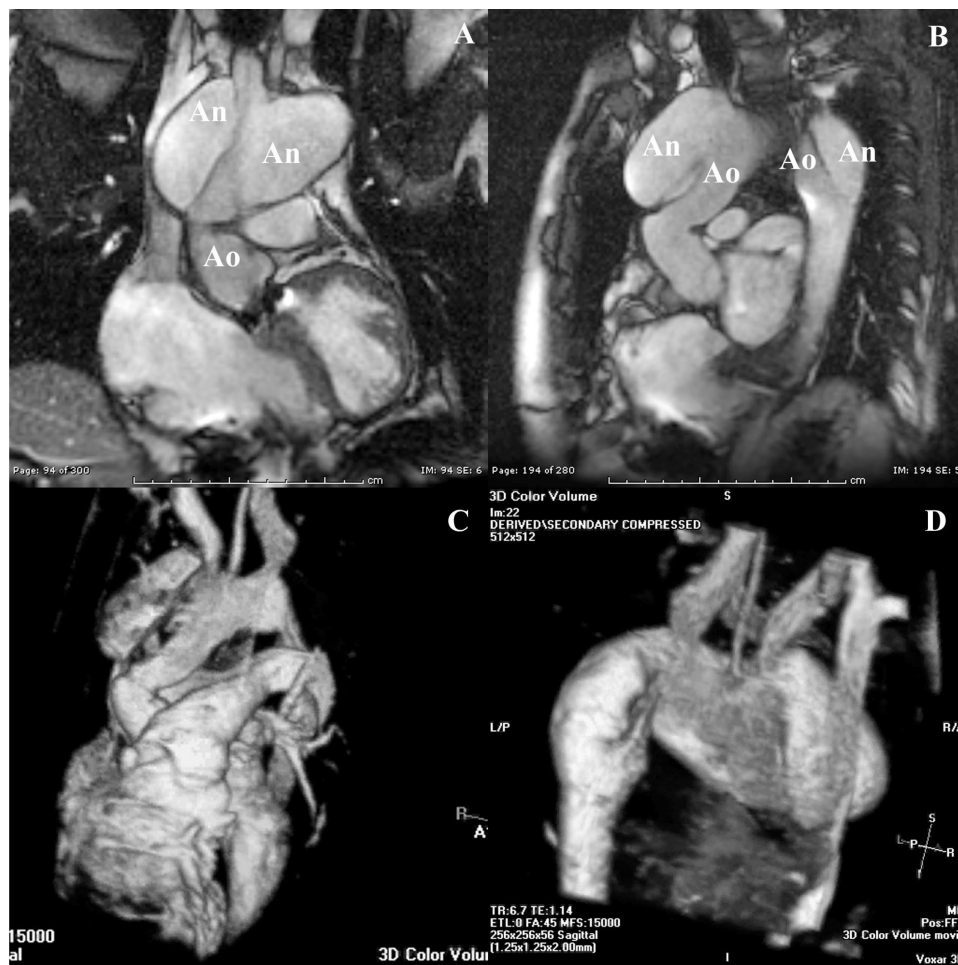


Figure 2. Patient with Marfan's syndrome status post aortic root replacement who presents with painless dissection. A) Single frame from steady state precession imaging in the coronal plane. "An" represents false aneurysm lumen. "Ao" represents true aortic lumen. B) Similar image in parasagittal orientation. C) 3D reconstruction of first phase of CEMRA (16 second acquisition, 8 second delay time). The tubular ascending graft is undisturbed but the native aortic lumen from the graft to the descending aortic is semilunar because of intimal dissection. Dissection passes through origins of the innominate and left subclavian artery and the entry point to the pseudoaneurysm is at the base of the innominate. D) 3D reconstruction of CEMRA taken immediately following the previous image (16 second acquisition). Contrast has cleared the native aorta but is retained in the giant pseudoaneurysm.

Not only does it offer high resolution static and dynamic imaging of stenoses, but CMR can assess the functional significance as well through phase-contrast volumetric flow measurements. This is critically important in a parallel circuit like the pulmonary arteries where one can have little significant pressure difference across a major obstruction.

Figure 3 demonstrates the utility of gradient-echo cine images in characterizing the hemodynamic significance of pulmonary stenoses. Patient was a 16-year-old patient with pulmonary atresia, ventricular septal defect, status post pulmonary homograft interposition from the right ventricle (RV) to the main pulmonary artery (MPA). Echocardiography revealed a peak velocity of 3.5 m/s in the pulmonary outflow by continuous wave Doppler. The MRI was ordered to determine level of obstruction and the degree of pulmonary insufficiency. Branch pulmonary arteries were previously thought to be normal on

echocardiogram. The homograft is observed to lie in a relatively orthotropic position (panel A) without kinks or sternal compression. However, valve leaflets are frozen inferiorly, creating a discrete systolic jet of turbulence (Panel B) that represents the primary source of the pressure drop predicted by echocardiography. Regurgitant fraction was <10% and the RV was not dilated (not shown) suggesting pure pressure load. This MR examination also demonstrated severe proximal left pulmonary artery (LPA) stenosis (panels C, D). Although the LPA completely abuts the MPA, communication only occurs through a 3 mm opening. A turbulent jet (independent from the MPA obstruction) is seen into the proximal LPA. By phase-contrast flow measurements, only 10% of the pulmonary blood flow reached the LPA. This patient was referred for LPA angioplasty with possible stent placement, rather than surgical replacement of the homograft.



Figure 3. Patient with pulmonary atresia, VSD status post pulmonary homograft placement. A, B) Single SPGR cine frame of left pulmonary artery in diastole and in systole, illustrating turbulent jet from proximal LPA stenosis. C, D) Single SPGR cine frame of RV to homograft connection. The homograft lies similarly to a native main pulmonary artery and is not compressed by the sternum or kinked. However, the inferior valve leaflets do not move restricting effective flow diameter by roughly 50%.

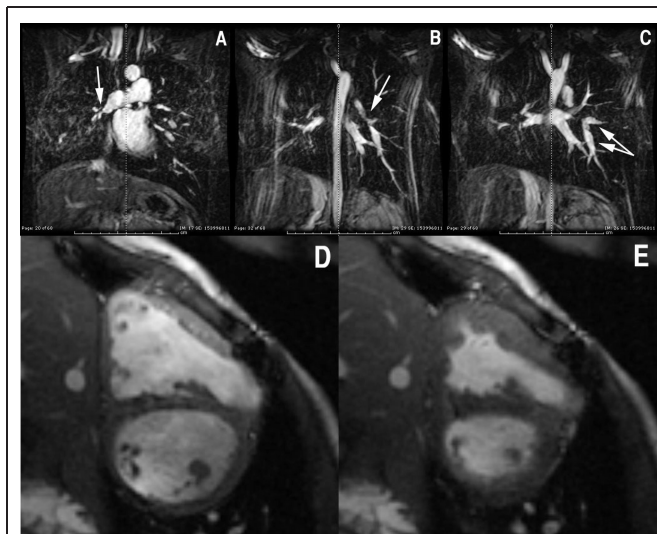


Figure 4. Patient with suspected Alagille's syndrome and peripheral pulmonary stenosis. 3D CEMRA in the coronal plane demonstrates massively dilated central pulmonary arteries with diffuse pulmonary arteriopathy in the second and third order branches. A) Near interruption of the RPA as it trifurcates into upper, middle, and lower branches (arrow). B, C) Alternating dilations and constrictions in the left lower pulmonary artery creates a "beaded" appearance to the vessel. D) Diastolic short axis cine SSFP image illustrating concentric RV hypertrophy and mild septal flattening (suggesting elevated RV end diastolic pressures). E) End-systolic frame of same sequence demonstrating pronounced *systolic* septal flattening as well, indicating high right ventricular systolic pressures.

Case 4: Peripheral pulmonary stenosis

Although white blood cine techniques work well for proximal stenoses, distal pulmonary obstruction is often best highlighted by CEMRA. Figure 4 demonstrates a 11-year-old patient with suspected Alagille's syndrome and peripheral pulmonary stenosis. Proximal PA's are very dilated (panels A–C) but prune immediately in second and third order branches. Both the right and left side are heavily involved. Vessels have an irregular, "beaded," appearance for alternating dilations and constrictions (arrows). The flow profile by phase contrast velocity measurements (not shown), often exhibits "ringing" and systolic prolongation. Right ventricular hypertrophic and systolic interventricular septal flattening suggest moderate stenosis (panels D, E).

Case 5: Pulmonary arteriovenous (AV) fistula

A relatively uncommon but interesting application of MRI in the pulmonary distribution is arteriovenous fistulae recognition. Figure 5 demonstrates images from an otherwise healthy 14-month-old boy with unexplained cyanosis. Contrast echocardiography demonstrated rapid left atrial filling with agitated saline injection peripherally but did not provide further insights. White blood cine imaging (panel A) demonstrates vascular nests in the posterior right lung with large "feeder" vessels and dilated right pulmonary artery (RPA). Slight involvement

of posterior left lung was also noted. Torrential blood flow was measured in the RPA by phase contrast velocity measurements (3.3 L/min/m^2). The bronchial distribution was grossly normal by black-blood imaging (panel B). To evaluate for possible early pulmonary venous return, the CEMRA was acquired with the center of k-space occurring within 4 or 5 seconds of injection. Image quality was suboptimal because of respiratory artifact and relatively little contrast delivery, however right pulmonary veins (RPV) are clearly delineated while left pulmonary veins remain unenhanced (panel C). The second phase of the angiogram (panel D) delineates the location and extent of the fistulous vessels in the posterior right lung. The posterior aspect of the left lung exhibits some minor changes as well, concordant with the cine imaging.

Pulmonary venous drainage

In addition to characterizing great artery location and stenoses, CMR is also ideally suited to evaluating the great veins (7, 14). These connections are usually easily defined by CEMRA in the coronal plane, however white blood cine imaging is often sufficient for diagnosis. The inability to distinguish between arteries, veins, and bronchial structures (except by tracking them) makes black-blood imaging generally less useful in pulmonary vein questions.

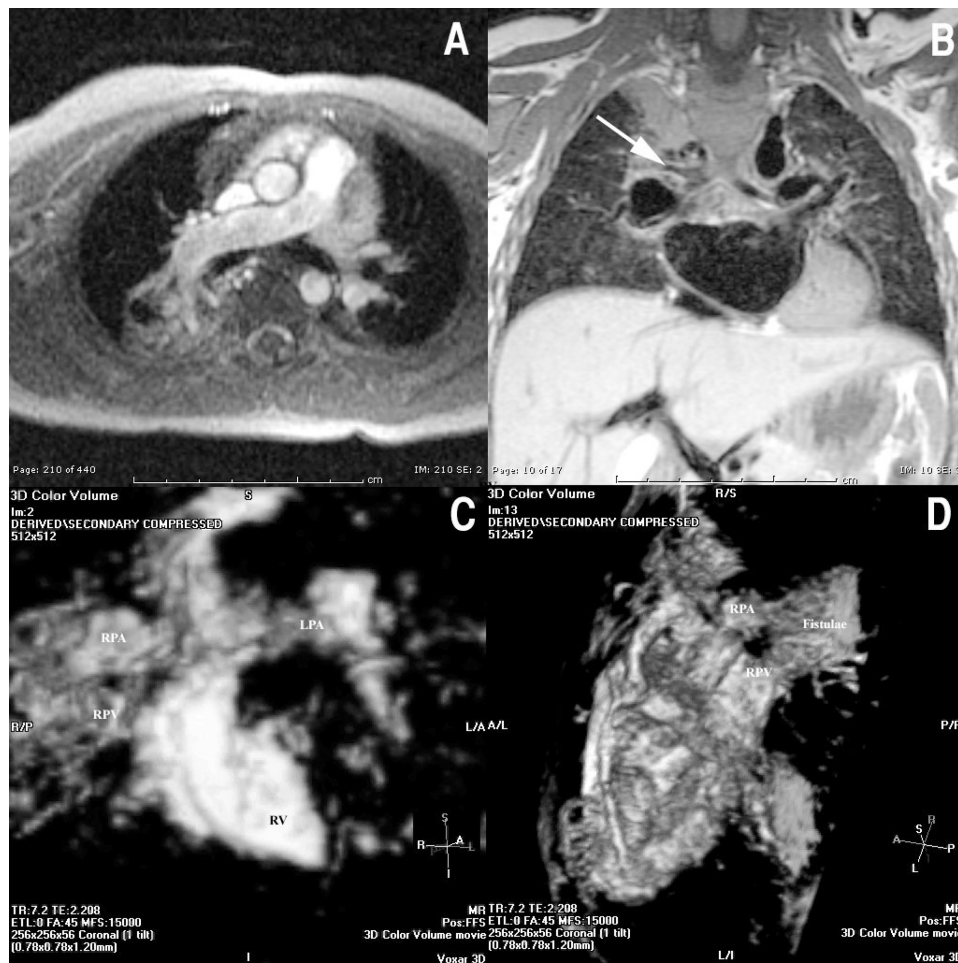


Figure 5. Four year old patient with persistent hypoxia and echocardiographic suggestion of pulmonary AV fistulae by contrast injection. A) Single frame of axial SPGR cine sequence demonstrated dilated right pulmonary artery, a large vascular “nest” posteriorly and larger feeder vessels. The abnormal region is clearly demarcated from the normal lung parenchyma by its general vascularity, B) Single spin echo black-blood image demonstrates the carina and first order bronchial branching on the right. The abnormal vessels are predominately confined to the upper lobe; C) First phase of the CEMRA opacifies the right pulmonary veins (RPV) even before the left pulmonary artery (LPA) is completely filled; D) The second phase of the CEMRA (postero-cranial angulation) demonstrates persistent contrast opacification of a ball of abnormal vessels posteriorly in the right lung (labeled fistula). Similar, but more subtle changes are seen in the posterior aspect of the left lung as well.

Case 6: Reobstruction of total anomalous pulmonary venous connection repair

The ability of SPGR to visualize flow acceleration (signal enhancement) and turbulence (signal void) is particularly helpful in evaluating pulmonary venous obstruction. Figure 6 demonstrates a complex restenosis seen in a 4 year old patient following repair of total anomalous venous connection in infancy. Diagnosis was suspected because of pulmonary hypertension and high-velocity jet observed in the left atrium by echocardiogram. Coronal SPGR demonstrates dilated proximal left and right pulmonary veins coming together at the surgical anastomosis site (panel A). Sagittal cuts from left to right (panels B–G) demonstrate tapering of the veins until they are functionally discontinuous from one another, with each vein communicating to the atria through a long slit-like surgical anastomosis.

Signal voids from both the left and right pulmonary vein flows project far into the left atrium, consistent with clinically-relevant obstruction.

Systemic venous drainage

Two dimensional MR imaging is superior to angiographic techniques, either invasive or noninvasive, for characterization of systemic venous abnormalities because it may be difficult or impossible to deliver effective contrast concentrations to the veins of interest. As a result, CMR is superior to echo and to cardiac catheterization for defining venous abnormalities for presurgical planning in heterotaxy patients (7). CEMRA may be a useful adjunct to two-dimensional imaging, particularly for defining veno-venous collaterals, but injection sites must be matched to the anatomic question.

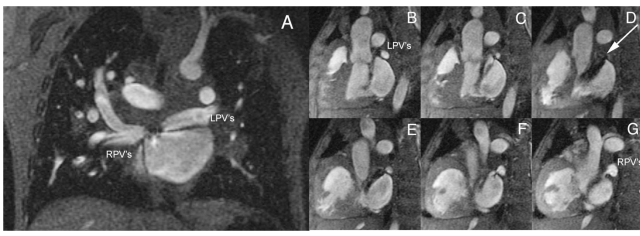


Figure 6. Four year old patient with total anomalous pulmonary venous drainage repaired in infancy. Coronal SPGR cine sequence (A) demonstrates dilated right and left pulmonary veins draining to the posterior aspect of the atrium. The anastomosis is better profiled by sagittal SPGR images collected from proximal left common pulmonary vein to proximal right common pulmonary vein (B–G). There is circumferential tapering of the proximal left and right portions of the veins (L > R) with functional separation between the two sides. Communication of the pulmonary vein confluence to the atrium has been reduced to a slit and there is a high velocity continuous jet spilling into the atrium.

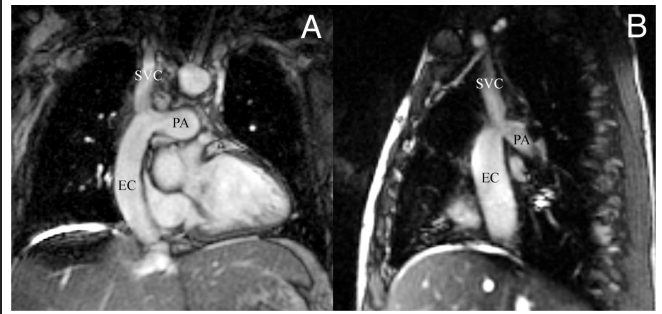


Figure 8. A) Single frame from coronal SSFP cine acquisition profiling superior and inferior venous connections in a Fontan patient. The external conduit (EC) passes along the anterolateral aspect of the right atrium. B) Single frame from sagittal SSFP cine acquisition profiling the same venous connections. Both SVC and EC connections have somewhat acute junctions with the right pulmonary artery. However, no flow turbulence is noted and the proximal vessels are not dilated.

Case 7: Membranous superior vena cava (SVC) obstruction

Anomalous systemic venous drainage is extremely common in CHD, particularly in patients with heterotaxy syndrome (7, 14). These abnormalities, as well as visceral situs abnormalities, are easily characterized by black-blood or white blood cine techniques. CEMRA has less utility in this regard because contrast generally follows the path of least resistance to the heart, although some retrograde venous perfusion may be seen with aggressive injection rates. Isolated great vein obstruction is most commonly iatrogenic (central venous catheter complications) but can rarely occur as isolated congenital defects. Figure 7 demonstrates a 1-year-old patient with known mild pulmonary valve stenosis who underwent an MRI to evaluate her branch pulmonary arteries (which were poorly profiled on echocardiography). The pulmonary arteries were unobstructed however, as an incidental finding, a high-grade stenosis was observed at the

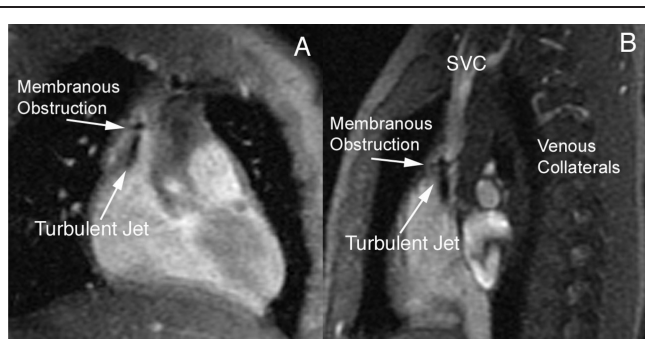


Figure 7. A) Single frame from coronal SPGR cine demonstrated a discrete membranous SVC obstruction at the junction to the right atrium. High velocity continuous single void is noted. B) Single frame from sagittal SPGR sequence profiling the orthogonal view. Paraspinal venous channels are unusually prominent, representing venous collateral flow.

junction between the superior vena cava and the right atrium. SPGR demonstrated a discrete tissue web and a high velocity turbulent jet extending into the right atrium. Sagittal views also demonstrated prominent venous collaterals along the spine. Because of the thin and mobile nature of this obstruction, this lesion was undetectable on the CEMRA, but was evident on gated black-blood imaging (not shown). Cardiac catheterization demonstrated a 12 torr mean gradient that was subsequently eliminated by balloon angioplasty.

Case 8: Failing Fontan

Systemic venous anastomoses are particularly important in evaluating patients who have undergone Fontan procedures. Since these patients tend to be older and have sluggish blood flow in the venous connections, SSFP techniques have clear advantages over SPGR. The following 15-year-old patient with protein losing enteropathy was referred to rule out Fontan circuit obstruction. Figure 8 demonstrates coronal and sagittal SSFP

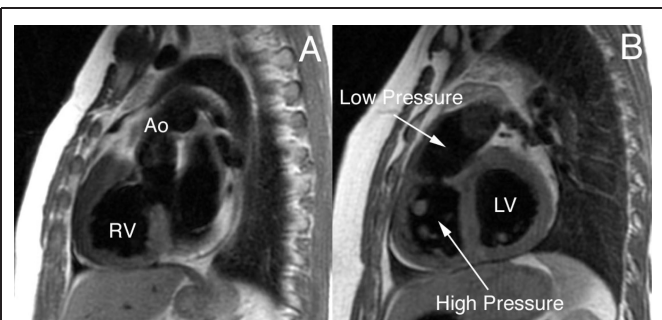


Figure 9. Sagittal double inversion recovery fast spin echo images from a patient with double chambered right ventricle. A) Large perimembranous VSD is noted without significant conal malignment. B) Thick, circumferential collar of fibromuscular tissue divides the right ventricle into high and low pressure chambers.

images of the Glenn and extracardiac Fontan connections. These connections are not offset in this patient although they enter at different angles. The SVC connection is somewhat tapered in the anterior-posterior dimension, but there is no SVC dilation proximally to suggest hemodynamic significance. The inferior vena cava (IVC) and hepatic veins were not dilated and the pulmonary arteries demonstrated no stenoses (not shown). The single ventricular function was mildly depressed. The patient was managed with aggressive afterload reduction.

Intracardiac Lesions

Case 9: Double chambered right ventricle

Although MRI is most useful for extracardiac abnormalities, it is also quite helpful in characterizing complex intracardiac relationships when echo views are restricted or inconclusive (23). For example, a 14 year patient presented with a clinical history and exam suggestive of double chambered right ventricle. The patient had very poor transthoracic acoustic windows and MRI is well suited for definitive diagnosis (24). Sagittal double inversion recovery FSE images (Figure 9) demonstrates a large membranous ventricular septal defect without significant conal malignment (panel A). A fibromuscular collar at the os-infundibulum divides the right ventricle in a high and low pressure chamber (panel B). Notice the difference in right ventricular thickness above and below the obstruction. The degree of hypertrophy suggests near systemic proximal RV pres-

ures and the patient was referred to surgery without additional studies.

Combination Lesions

Case 10: Truncus arteriosus

The last two examples highlight the comprehensive nature of CMR in evaluating congenital cardiac abnormalities. Figure 10 demonstrates a neonate with truncus arteriosus who was referred because echocardiograms did not completely define the great artery anatomy. The common trunk (panel A) appears to be doubly-committed to the right and left ventricle. This relationship is important because occasionally the common trunk will arise predominately from the right ventricle with a fairly shallow ventricular septal defect as the only systemic egress. The aorta emerges at a 45° angle from the right side of the common trunk (panel B, C) but otherwise has a normal left aortic arch course and branching pattern (panels C, D). The right pulmonary arises from the left side of the common trunk and swings posterior to the trunk to enter the right hilum (panel E), while the left pulmonary artery represents the posterior continuation of the common trunk (panel C–E). Cine gradient echo imaging demonstrated mild stenosis and regurgitation of the truncal valve (not shown) as well as evidence of torrential overcirculation. Notice the tense, displaced atrial septum, dilated left atrial appendage (LAA) and pulmonary veins (PV), and generous pulmonary

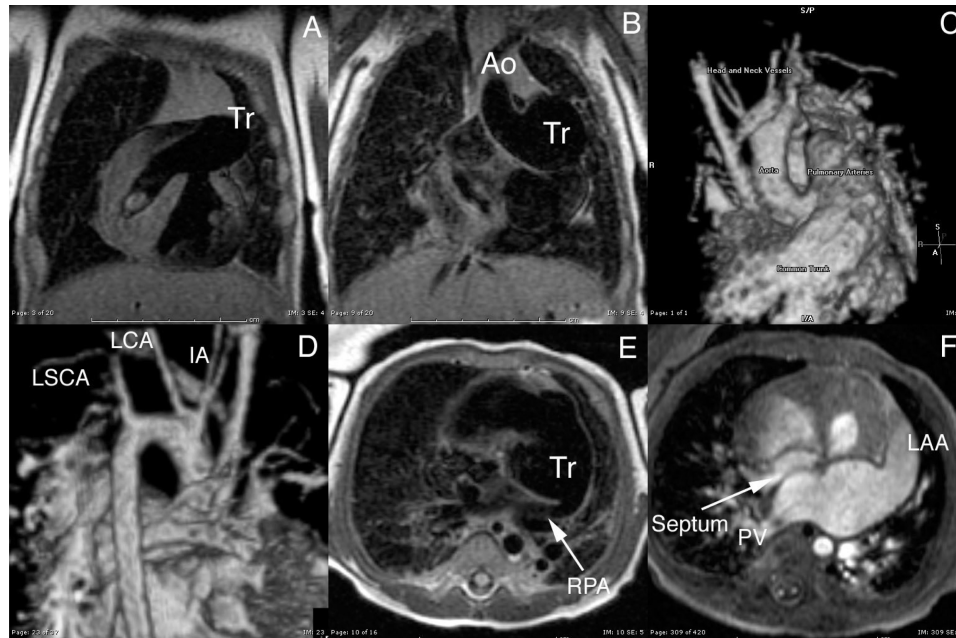


Figure 10. Patient with type 1 truncus arteriosus. A) Coronal T1 spin echo image demonstrating the truncal valve (Tr) orientation to malalignment ventricular septal defect. B) Similar image highlighting aortic takeoff at a 45° angle from the right side of the common trunk. The LPA represents continuation of the common trunk posteriorly. C, D) 3D rendering of CEMRA demonstrating a normal left aortic arch projecting from the right side of the common trunk. E) RPA arising from the left side of the common trunk and circling posteriorly. F) Axial cine image depicting tense pulmonary veins, atrial appendage, and deviated, intact, deviated, atrial septum as a result of torrential pulmonary blood flow.

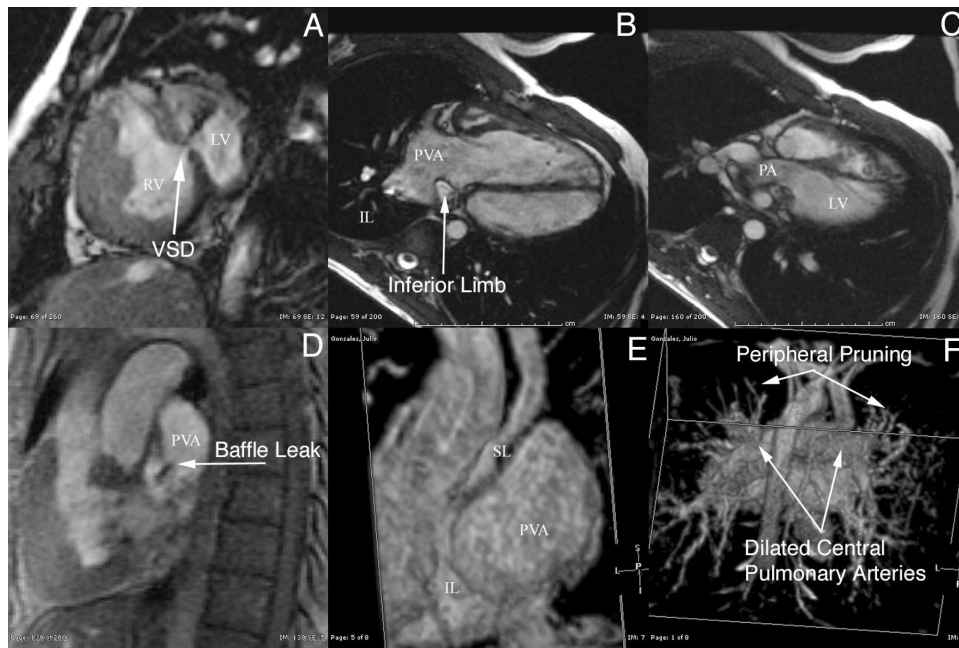


Figure 11. Transposition of the great arteries s/p Mustard procedure. A) Residual ventricular septal defect (VSD) with left to right shunt is well-profiled by cine SPGR. B) Unobstructed pulmonary venous atrial (PVA) connection to tricuspid valve (cine SSFP). C) No dynamic obstruction of left ventricular outflow tract is seen (cine SSFP). D) Small baffle leak is seen between the pulmonary venous atrium (PVA) and the systemic venous atrium. E) 3D angiogram reconstruction showing the superior and inferior limbs of the systemic venous baffle compared with the dilated pulmonary venous atrium. The superior limb tapers gradually but there is no great obstruction. F) Posterior view of 3D angiogram demonstrating dilated central pulmonary arteries with pruned distal vasculature, consistent with pulmonary vasculature disease.

vasculature from torrential left-to-right shunting (panel F). The patient was taken to surgery without further imaging.

Case 11: Transposition of the great arteries status post Mustard procedure

The final example is a 21-year-old patient with transposition of the great arteries with ventricular septal defect who underwent Mustard procedure at 6 months of age. The purpose for the MRI was decreasing exercise tolerance and poor intracardiac visualization by echocardiogram. Our protocol consisted of localizers, 4 chamber and short axis SSFP images, sagittal SPGR images, phase contrast velocity measurements in aorta and pulmonary artery and a CEMRA in the coronal plane. Short axis SSFP images demonstrated biventricular hypertrophy with preserved systolic function. A small residual ventricular septal defect was profiled with turbulent right ventricular (RV) to left ventricular (LV) shunting (panel A). Total pulmonary to systemic blood flow ratio, or Q_p/Q_s , for this patient was 1.2:1 by phase contrast flow measurements. Four chamber SSFP images demonstrated wide open pulmonary venous atrial (PVA) connection (panel B) and left ventricle to pulmonary artery (PA) outflow (panel C). Sagittal SPGR images demonstrated a small baffle leak (panel D) and unobstructed inferior systemic venous baffle (not shown). The superior limb of the atrial baffle tapered as it passed through the atrium with mild flow acceleration and no turbulence (not shown). The SVC tapering was also captured

by the CEMRA (panel E). The pulmonary vasculature was quite abnormal by CEMRA with dilated proximal PAs and pruned distal vessels (panel F). This represents irreversible vascular disease from the relatively late surgical repair. It is concordant with the mild LV hypertrophy present despite lack of any significant LV outflow tract obstruction. This example demonstrates how seamlessly CMR blends anatomic and functional characterization of a CHD patient's pathophysiology. Recent work also suggests the delayed gadolinium enhancement of the systemic right ventricle, perhaps serving as a surrogate marker for myocardial fibrosis, correlates with right ventricular failure and arrhythmias in adult atrial switch patients (25). Since poor exercise tolerance and ventricular failure represent a final common pathway for many forms of CHD (26), delayed hyperenhancement imaging may provide significant prognostic information for adults with CHD.

SUMMARY AND CONCLUSION

CMR is a powerful tool for complete characterization of congenital anatomy. Black-blood, white blood cine and 3D angiography offer complementary insights into congenital pathophysiology. Black-blood imaging offers superior resolution, contrast, and decreased sensitivity to metal artifacts. White blood cine imaging provides physiologic context to the anatomy, demonstrating flow patterns, valve motion, qualitative assessment of stenosis/regurgitation, and cardiac function. CEMRA offers

superb depiction of small vessel disease while also yielding the best three-dimensional representations of vessel relationships. Taken together, these tools can answer many questions formerly studied by diagnostic catheterization. Although echocardiography remains the primary initial diagnostic in infants and children, CMR may become that standard of care in patients with poor acoustic windows, such as adults with CHD.

REFERENCES

1. Tworetzky W, McElhinney DB, Brook MM, Reddy VM, Hanley FL, Silverman NH. Echocardiographic diagnosis alone for the complete repair of major congenital heart defects. *J Am Coll Cardiol* 1999;33:228–33.
2. Powell AJ, Maier SE, Chung T, Geva T. Phase-velocity cine magnetic resonance imaging measurement of pulsatile blood flow in children and young adults: in vitro and in vivo validation. *Pediatr Cardiol*. 2000;21:104–10.
3. Nield LE, Qi XL, Valsangiacomo ER, Macgowan CK, Wright GA, Hornberger LK, Yoo SJ. In vivo MRI measurement of blood oxygen saturation in children with congenital heart disease. *Pediatr Radiol* 2005;35:179–85.
4. Korperich H, Gieseke J, Barth P, Hoogeveen R, Esdorn H, Peterschroder A, Meyer H, Beerbaum P. Flow volume and shunt quantification in pediatric congenital heart disease by real-time magnetic resonance velocity mapping: a validation study. *Circulation* 2004;109:1987–93.
5. Prakash A, Powell AJ, Krishnamurthy R, Geva T. Magnetic resonance imaging evaluation of myocardial perfusion and viability in congenital and acquired pediatric heart disease. *Am J Cardiol* 2004;93:657–61.
6. Fleenor JT, Weinberg PM, Kramer SS, Fogel M. Vascular rings and their effect on tracheal geometry. *Pediatr Cardiol* 2003;24:430–5.
7. Geva T, Vick GW, 3rd, Wendt RE, Rokey R. Role of spin echo and cine magnetic resonance imaging in presurgical planning of heterotaxy syndrome. Comparison with echocardiography and catheterization. *Circulation* 1994;90:348–56.
8. Rebergen SA, Niezen RA, Helbing WA, van der Wall EE, de Roos A. Cine gradient-echo MR imaging and MR velocity mapping in the evaluation of congenital heart disease. *Radiographics* 1996;16:467–81.
9. Pereles FS, Kapoor V, Carr JC, Simonetti OP, Krupinski EA, Baskaran V, Finn JP. Usefulness of segmented trueFISP cardiac pulse sequence in evaluation of congenital and acquired adult cardiac abnormalities. *Am J Roentgenol* 2001;177:1155–60.
10. Markl M, Pelc NJ. On flow effects in balanced steady-state free precession imaging: pictorial description, parameter dependence, and clinical implications. *J Magn Reson Imaging* 2004;20:697–705.
11. Powell AJ, Chung T, Landzberg MJ, Geva T. Accuracy of MRI evaluation of pulmonary blood supply in patients with complex pulmonary stenosis or atresia. *Int J Card Imaging* 2000;16:169–74.
12. Prasad SK, Soukias N, Hornung T, Khan M, Pennell DJ, Gatzoulis MA, Mohiaddin RH. Role of magnetic resonance angiography in the diagnosis of major aortopulmonary collateral arteries and partial anomalous pulmonary venous drainage. *Circulation* 2004;109:207–14.
13. Geva T, Greil GF, Marshall AC, Landzberg M, Powell AJ. Gadolinium-enhanced 3-dimensional magnetic resonance angiography of pulmonary blood supply in patients with complex pulmonary stenosis or atresia: comparison with x-ray angiography. *Circulation* 2002;106:473–8.
14. Greil GF, Powell AJ, Gildein HP, Geva T. Gadolinium-enhanced three-dimensional magnetic resonance angiography of pulmonary and systemic venous anomalies. *J Am Coll Cardiol* 2002;39:335–41.
15. Greenberg SB, Bhutta ST, Buchmann RF. Gadolinium-enhanced magnetic resonance angiography in neonates and infants suspected of caval or aortic thrombosis. *Pediatr Radiol* 2004;34:948–51.
16. Carr JC, Laub G, Zheng J, Pereles FS, Finn JP. Time-resolved three-dimensional pulmonary MR angiography and perfusion imaging with ultrashort repetition time. *Acad Radiol* 2002;9:1407–18.
17. Tsai-Goodman B, Geva T, Odegard KC, Sena LM, Powell AJ. Clinical role, accuracy, and technical aspects of cardiovascular magnetic resonance imaging in infants. *Am J Cardiol* 2004;94:69–74.
18. Odegard KC, DiNardo JA, Tsai-Goodman B, Powell AJ, Geva T, Laussen PC. Anaesthesia considerations for cardiac MRI in infants and small children. *Paediatr Anaesth* 2004;14:471–6.
19. Tatli S, Yucel E, Lipton M. T and MR imaging of the thoracic aorta: current techniques and clinical applications. *Radiol Clin North Am* 2004;42:565–8.
20. Nielsen JC, Powell AJ, Gauvreau K, Marcus EN, Prakash A, Geva T. Magnetic resonance imaging predictors of coarctation severity. *Circulation* 2005;111:622–8.
21. Araoz PA, Reddy GP, Tarnoff H, Roge CL, Higgins CB. MR findings of collateral circulation are more accurate measures of hemodynamic significance than arm-leg blood pressure gradient after repair of coarctation of the aorta. *J Magn Reson Imaging* 2003;17:177–83.
22. Bornemeier RA, Weinberg PM, Fogel MA. Angiographic, echocardiographic, and three-dimensional magnetic resonance imaging of extracardiac conduits in congenital heart disease. *Am J Cardiol* 1996;78:713–7.
23. Fogel MA, Hubbard A, Weinberg PM. A simplified approach for assessment of intracardiac baffles and extracardiac conduits in congenital heart surgery with two- and three-dimensional magnetic resonance imaging. *Am Heart J* 2001;142:1028–36.
24. Kilner PJ, Sievers B, Meyer GP, Ho SY. Double-chambered right ventricle or sub-infundibular stenosis assessed by cardiovascular magnetic resonance. *J Cardiovasc Magn Reson* 2002;4:373–9.
25. Babu-Narayan SV, Goktekin O, Moon JC, Broberg CS, Pantely GA, Pennell DJ, Gatzoulis MA, Kilner PJ. Late gadolinium enhancement cardiovascular magnetic resonance of the systemic right ventricle in adults with previous atrial redirection surgery for transposition of the great arteries. *Circulation* 2005;111:2091–8.
26. Diller GP, Dimopoulos K, Okonko D, Li W, Babu-Narayan SV, Broberg CS, Johansson B, Bouzas B, Mullen MJ, Poole-Wilson PA, Francis DP, Gatzoulis MA. Exercise intolerance in adult congenital heart disease: comparative severity, correlates, and prognostic implication. *Circulation* 2005;112:828–35.